Analysis for Free Dendritic Growth Model Applicable to Nondilute Alloys

SHU LI, JIONG ZHANG, and PING WU

A steady-state free dendritic growth model applicable to concentrated alloys was proposed as an extension of Wang *et al.*'s model.[14] The present model adopted a realistic thermodynamic model to replace the Baker–Cahn equation and included a generalized marginal stability criterion and a nondilute solute trapping model to completely eliminate the dilute alloy limitation. Comparative analysis shows that Wang *et al.*'s model is a very close approximation to the present model at low undercoolings for dilute alloys. However, the difference appears at high undercoolings even for dilute alloys. Furthermore, the difference of the model predictions for both models increases with nominal composition of alloys due to the inherent limitation of dilute alloys in Wang *et al.*'s model. A comparison with the experimental data for $Cu_{70}Ni_{30}$ alloy demonstrates the applicability of the present model to nondilute alloys.

DOI: 10.1007/s11661-012-1189-2
© The Minerals, Metals & Materials Society and ASM International 2012

I. INTRODUCTION

THE free dendritic growth in an undercooled alloy melt as a main subject in the research of solidification theory has fueled increasing attention in past decades.[1–3] In the original free dendritic growth model (LGK model),[4] Lipton *et al.* assumed local equilibrium condition with no interfacial kinetic effect and adopted a morphological stability criterion along with an equation for the total undercooling to predict the radius of curvature and the velocity at the tip. In order to describe high Péclet number conditions, *i.e.*, deviations from the local-equilibrium state, some models[5–8] were proposed later. Among them, the Boettinger–Coriell–Trivedi (BCT) model[7] received wide acceptance due to its relative simplicity as well as the ability to describe rapid solidification by introducing the thermodynamic driving force, the kinetic undercooling, and Aziz's solute trapping model.

Several simplifying assumptions, however, restrict the application of the BCT model. One of them is the assumption of straight solidus and liquidus. It leads to a significant discrepancy in model predictions for alloys with the retrograde-type solidus and curved liquidus. Divenuti and Ando eliminated this limitation and developed a model (DA model)[8] with curved (real) phase boundaries, based on the BCT model. Another assumption in the BCT model is the equilibrium solute diffusion in bulk liquid. That is the BCT model does not take into account the relaxation effect of nonequilibrium liquid diffusion, which is supported by experiments[9–11] and theories.[12] Galenko and Danilov (GD model)[13] and Wang *et al.*[14] incorporated the relaxation effect into the BCT model with and without linear phase boundary assumptions, respectively. These two models have a finite value for the solutal diffusion velocity in bulk liquid in contrast with the previous models, in which the relaxation time is neglected and thus the diffusion velocity is infinite.

All of the preceding models are restricted to dilute alloys. Consequently, the range of application is limited. Most importantly, the dilute assumption can bring on remarkable deviations under certain conditions. This was demonstrated for planar interface migration[15] and marginal stability criterion.[16] Recently, Önel and Ando[17] modified the DA model by using a thermodynamic solution model to replace the Baker–Cahn equation limited by Henry's law. Also, Hartmann *et al.*[18] introduced a nondilute solute trapping equation into the GD model to describe the solidification behavior for $Ti_{45}Al_{55}$ alloy. However, these modifications are partial and incomplete. In this study, a steady-state free dendritic growth model, which is applicable to nondilute alloys, was proposed as an extension of Wang *et al.*'s model. The present model is self-consistent since it revised all three parts of the free dendritic growth model, namely, the interfacial driving force, the marginal stability criterion, and the solute trapping equation. A comparison with Wang *et al.*'s model and the available experimental data was also made.

II. MODEL

A. *Interfacial Driving Force*

Founded on Galenko's extended irreversible thermodynamic analysis[19] for migration of a solid/liquid

SHU LI, Associate Professor, is with the College of Applied Science, Harbin University of Science and Technology, Harbin 150080, Heilongjiang, People's Republic of China. JIONG ZHANG, formerly Undergraduate Student with the Tianjin Key Laboratory of Low Dimensional Materials Physics and Preparing Technology, Department of Applied Physics, Institute of Advanced Materials Physics, School of Science, Tianjin University, Tianjin 300072, People's Republic of China, is now Graduate Student with the Department of Physics and Astronomy, University of Missouri-Columbia, Columbia, MO 65201. PING WU, Professor, is with the Tianjin Key Laboratory of Low Dimensional Materials Physics and Preparing Technology, Department of Applied Physics, Institute of Advanced Materials Physics, School of Science, Tianjin University. Contact e-mail: pingwu@tju.edu.cn

Manuscript submitted May 11, 2009.
Article published online June 13, 2012

interface, the interfacial driving force (ΔG_{eff}) applicable to nondilute alloys can be derived as[15]

$$\Delta G_{\text{eff}} = (1 - C^*) \cdot \Delta\mu_1 + C^* \cdot \Delta\mu_2 - \gamma(C_l^* - C_s^*)^2 \times \left[(1 - C_l^*)\frac{\partial \mu_2^l}{\partial C_l^*} + C_l^* \frac{\partial \mu_1^l}{\partial (1 - C_l^*)}\right] \frac{V}{V_D}, \quad V < V_D \qquad [1a]$$

$$\Delta G_{\text{eff}} = \left(1 - C_s^*\right) \cdot \Delta\mu_1 + C_s^* \cdot \Delta\mu_2, \quad V \geq V_D \qquad [1b]$$

where subscripts 1 and 2 denote solvent and solute, respectively, for a binary alloy solution; scripts l and s represent liquid and solid phases, respectively; μ is the chemical potential; $\Delta\mu$ is the change in μ upon solidification ($\mu^s - \mu^l$); V is the interface migration velocity; V_D is the solutal diffusion velocity in bulk liquid; and C_s^* and C_l^* are the solute concentrations at the interface and $C^* = (1 - \gamma)C_s^* + \gamma C_l^*$, respectively. The parameter γ is introduced to unify both forms of ΔG_{eff} without ($\gamma = 0$) and with ($\gamma = 1$) solute drag. And the values $0 \sim 1$ of γ indicate the forms with partial solute drag. The so-called solute drag[20–22] refers to a phenomenon that a part of total Gibbs free energy change in solidification is dissipated by the solute-solvent redistribution and is not available to drive interfacial motion. It leads to slowing of the interfacial migration.

The last term in Eq. [1a] is the change of free energy corresponding to local nonequilibrium diffusion caused by the relaxation effect. This term disappears when $V \geq V_D$ due to the occurrence of partitionless solidification. For dilute alloys, Eqs. [1a] and [1b] with $\gamma = 1$ reduce to Galenko's result[19] on the assumption of linear phase boundaries and reduce to the following expressions used in Wang *et al.*'s model with real solidus and liquidus:[14]

$$\frac{\Delta G_{\text{eff}}}{\mathrm{R_g} T_i} = C_s^{eq'} - C_l^{eq'} + C_l^* \left[1 - k + \ln\left(\frac{k}{k_e'}\right) + (1 - k)^2 \frac{V}{V_D}\right], \quad V < V_D \qquad [2a]$$

$$\frac{\Delta G_{\text{eff}}}{\mathrm{R_g} T_i} = C_s^{eq'} - C_l^{eq'} - C_l^* \ln k_e', \quad V \geq V_D \qquad [2b]$$

where $C_l^{eq'}$ and $C_s^{eq'}$ are the curvature modified equilibrium solute concentrations in the liquid and solid, respectively, at the interface; k_e' is the curvature modified equilibrium partition coefficient ($k_e' = C_s^{eq'}/C_l^{eq'}$); k is the nonequilibrium partition coefficient; $\mathrm{R_g}$ is the gas constant; and T_i is the interfacial temperature. In the two expressions, the chemical potential differences, $\Delta\mu_1$ and $\Delta\mu_2$, were replaced by the results from Baker and Cahn:[23]

$$\Delta\mu_1 = \mathrm{R_g} T_i \ln \frac{(1 - C_s^*)(1 - C_l^{eq'})}{(1 - C_l^*)(1 - C_s^{eq'})} = \mathrm{R_g} T_i (C_l^* - C_s^* + C_s^{eq'} - C_l^{eq'}) \qquad [3a]$$

$$\Delta\mu_2 = \mathrm{R_g} T_i \ln\left(\frac{k}{k_e'}\right) \qquad [3b]$$

where an approximation ($\ln(1 + x) \approx x$, in Eq. [3a]) is adopted to further simplify Baker and Chan's results. Note that for the phase diagrams of most alloy systems, the equilibrium solute concentration $C_l^{eq'}$ is not suitable for the approximation $\ln(1 - C_l^{eq'}) \approx -C_l^{eq'}$ at high undercoolings, *i.e.*, low interfacial temperatures. Therefore, the application of Wang *et al.*'s model is considerably limited. For the interfacial driving force, a detailed comparative analysis of the present model and other typical models including Wang *et al.*'s model can be found in Reference 15.

According to Turnbull's chemical rate theory,[24] ΔG_{eff} can be related to V as

$$\Delta G_{\text{eff}}(V, T_i + \Delta T_r, C_l^*)/\mathrm{R_g}(T_i + \Delta T_r) - \ln(1 - V/fV_0) = 0 \qquad (4)$$

where f is the site fraction for growth to occur at the interface, V_0 is the maximum crystallization velocity, and ΔT_r is the curvature undercooling caused by the Gibbs–Thompson effect. Different from the planar interface migration, the curvature correction is necessary for dendritic growth.[7,8]

B. *Marginal Stability Criterion*

In previous work, a generalized marginal stability theory for a planar interface during solidification was proposed.[16] In this section, the aim is to describe the curvature radius r at the tip (curved interface) during dendritic solidification. This is also based on the generalized marginal stability theory.[16]

For an unperturbed (planar) interface, the curvature effect disappears and the interface response function, Eq. [4], reduces to

$$\Delta G_{\text{eff}}(V, T_i, C_f)/\mathrm{R_g} T_i - \ln(1 - V/fV_0) = 0 \qquad [5]$$

where C_f is the liquid composition at the planar interface. Assuming this interface is subjected to an infinitesimal sinusoidal perturbation $\phi = \delta(t) \sin \omega x$, where δ is the perturbed amplitude, ω is the perturbed wave number, t is time, and x is the interfacial position, Eq. [5] is then rewritten as

$$\Delta G_{\text{eff}}(V^\phi, T_i^\phi + \Gamma\omega^2\delta \sin \omega x, C_f^\phi)/\mathrm{R_g}(T_i^\phi + \Gamma\omega^2\delta \sin \omega x) - \ln(1 - V^\phi/fV_0) = 0 \qquad [6]$$

where $\Gamma\omega^2\delta \sin \omega x$ represents the curvature undercooling ΔT_r; Γ is the Gibbs–Thompson coefficient; and V^ϕ, T_i^ϕ, and C_f^ϕ are the migration velocity, the temperature, and the liquid composition, respectively, corresponding to the perturbed interface. They are linearly approximated by

$$T_i^\phi = T_i + a\delta \sin \omega x = T_i + a\phi \qquad [7a]$$

$$C_f^\phi = C_f + b\delta \sin \omega x = C_f + b\phi \qquad [7b]$$

$$V^\phi = V + \dot{\delta} \sin \omega x \qquad [7c]$$

Combining Eqs. [5] and [7] with the first-order approximation to Eq. [6], one obtains the following stability equation:

$$a = -\Gamma\omega^2 + M(V, T_i + \Delta T_r, C_f)b - \frac{\dot{\delta}}{\delta}\frac{1}{\mu^*} \quad [8]$$

where $M(V, T_i + \Delta T_r, C_f)$ is regarded as the kinetic liquidus slope defined by

$$M(V, T_i + \Delta T_r, C_f) = \frac{-C}{B - \mathrm{R_g}\ln(1 - V/fV_0)} \quad [9]$$

and the related parameters are given as

$$\frac{1}{\mu^*} = \frac{A + \mathrm{R_g}(T_i + \Delta T_r)/(fV_0 - V)}{B - \mathrm{R_g}\ln(1 - V/fV_0)} \quad [10]$$

$$A = \left.\frac{\partial \Delta G_{\mathrm{eff}}(V_x, T_i + \Delta T_r, C_f)}{\partial V_x}\right|_{V_x = V} \quad [11a]$$

$$B = \left.\frac{\partial \Delta G_{\mathrm{eff}}(V, T_x, C_f)}{\partial T_x}\right|_{T_x = T_i + \Delta T_r} \quad [11b]$$

$$C = \left.\frac{\partial \Delta G_{\mathrm{eff}}(V, T_i + \Delta T_r, C_x)}{\partial C_x}\right|_{C_x = C_f} \quad [11c]$$

The kinetic liquidus slope $M(V, T_i + \Delta T_r, C_f)$ would reduce to $M(V, T_i + \Delta T_r)$, which is used in Wang *et al.*'s model,[14] if C_f is separated.

Solving the steady-state thermal and non-Fickian solutal diffusion equations (Eqs. [18] through [20] in Reference 14) around a perturbed interface, and combining the boundary conditions on the perturbed interface (transport balances (Eq. [34] in Reference 14)), one yields the constant values of a and b. Consequently, from Eq. [8], the marginal stability criterion for dendritic growth can be obtained as (C_f is replaced by C_l^*)

$$-\Gamma\omega^2 - \frac{1}{2}G_l\xi_l - \frac{1}{2}G_s\xi_s + M(V, T_i + \Delta T_r, C_l^*)G_c\xi_c = 0 \quad [12]$$

where

$$\xi_l = 1 - \frac{1}{\sqrt{1 + (\sigma^* P_t^2)^{-1}}} \quad [13]$$

$$\xi_s = 1 + \frac{1}{\sqrt{1 + (\sigma^* P_t^2)^{-1}}} \quad [14]$$

$$\xi_c = 0, \quad V \geq V_D \quad [15b]$$

$$G_c = C_l^*(k - 1)V/D\psi, \quad V < V_D \quad [16a]$$

$$G_c = 0, \quad V \geq V_D \quad [16b]$$

in which $\psi = 1 - V^2/V_D^2$; σ^* is the stability constant ($\sigma^* \approx 1/4\pi^2$);[25] $P_t = rV/2\alpha$ is the thermal Péclet number; $P_c = rV/2D$ is the solute Péclet number; α and D are the thermal diffusivity and solute diffusion coefficient, respectively, in the liquid; and G_c is the solutal concentration gradient at interface in the liquid.[14] In addition, G_l and G_s are the thermal gradients at interface in the liquid and solid, respectively. Generally, G_s is negligible; *i.e.*, $G_s = 0$. From the boundary condition $K_s G_s - K_l G_l = \Delta H_f V$, G_l is then given as

$$G_l = -\Delta H_f V/K_l = -2\Delta H_f P_t/rC_p \quad [17]$$

where K_s and K_l are the thermal conductivities of solid and liquid, ΔH_f is the latent heat of fusion, and C_p is the heat capacity of liquid alloy.

According to Langer and Muller-Krumbhaar, the radius of curvature r at the dendritic tip can be approximated by the perturbed wavelength $\lambda(\lambda = 2\pi/\omega)$ with the marginal stability.[25] Consequently, from the marginal stability criterion Eq. [12], the expression of r is obtained as follows:[8,14,25–27]

$$r = \frac{\Gamma/\sigma^*}{\frac{P_t \Delta H_f}{C_p}\xi_t + \frac{2M(V, T_i + \Delta T_r, C_l^*)(k-1)C_l^* P_c}{\psi}\xi_c}, \quad V < V_D \quad [18a]$$

$$r = \frac{\Gamma/\sigma^*}{\frac{P_t \Delta H_f}{C_p}\xi_t}, \quad V \geq V_D \quad [18b]$$

The expression of ξ_t (ξ_l) is the same as that used in the previous models[5–8,13,14] except for the LGK model, in which an approximation to a small thermal Péclet number P_t is made. This is due to the fact that all the models are based on the same thermal diffusion equation (Eqs. [18] and [19] in Reference 14). However, there are differences in ξ_c between these models. In contrast with Wang *et al.*'s model, the present model includes an additional term $2C_l^*\partial k/\partial C|_{C=C_l^*}$ in ξ_c. This is because the present model considers the dependency of the nonequilibrium partition coefficient k on the interface solute concentration C_l^* (Eq. [20]). Furthermore, ξ_c used in Wang *et al.*'s model reduces to that of the GD model on the assumption of the linear phase boundaries (neglect the dependency of k on T_i) and reduces to that of the BCT model if the relaxation effect is neglected further.

$$\xi_c = 1 - \frac{2k + 2M(V, T_i + \Delta T_r, C_l^*)C_l^*\partial k/\partial T\big|_{T=T_i+\Delta T_r} + 2C_l^*\partial k/\partial C\big|_{C=C_l^*}}{\sqrt{1 + \psi(\sigma^* P_c^2)^{-1}} + 2k - 1 + 2M(V, T_i + \Delta T_r)C_l^*\partial k/\partial T\big|_{T=T_i+\Delta T_r} + 2C_l^*\partial k/\partial C\big|_{C=C_l^*}}, \quad V < V_D \quad [15a]$$

C. *Solute Trapping Equation*

For dilute alloys, including the relaxation effect of nonequilibrium liquid diffusion, the modified Aziz solute trapping equation is given as:[28]

$$k = \frac{\psi k'_e + V/V_{DI}}{\psi + V/V_{DI}}, \quad V < V_D \qquad [19a]$$

$$k = 1, \quad V \geq V_D \qquad [19b]$$

where V_{DI} is the interfacial solute diffusive speed defined by D_i/a_0, D_i is the solute diffusion coefficient at the interface, and a_0 is the interface width.

For nondilute alloys, Eq. [19] used in Wang *et al.*'s model needs to be extended. Galenko developed an extended description of the solute partition coefficient, which is well suitable for concentrated alloys:[29]

$$k = \frac{\psi \kappa'_e + V/V_{DI}}{\psi(1-(1-\kappa'_e)C^*_l) + V/V_{DI}}, \quad V < V_D \qquad [20a]$$

$$k = 1, \quad V \geq V_D \qquad [20b]$$

where κ'_e is the curvature corrected partitioning parameter defined by[20]

$$\kappa'_e(C^*_l, C^*_s, T_i + \Delta T_r) = \frac{C^*_s(1-C^*_l)}{C^*_l(1-C^*_s)} \exp[-(\Delta\mu_2 - \Delta\mu_1)/R(T_i + \Delta T_r)] \qquad [21]$$

D. *Ivantsov Treatments*

Ivantsov assumed that the interface exhibits a dendritic morphology with a paraboloid of revolution (near the tip), and the chemical composition and the temperature are constant along the interface. Solving the steady-state thermal and solutal diffusion equations in the liquid phase from the interface to infinite, Ivantsov obtained the dimensionless thermal undercooling Ω_t and the dimensionless supersaturation Ω_c, respectively:[30,31]

$$\Omega_t = \frac{C_p(T_i - T_\infty)}{\Delta H_f} = \mathrm{Iv}(P_t) \qquad [22]$$

$$\Omega_c = \frac{C^*_l - C_0}{C^*_l - C^*_s} = \mathrm{Iv}(P_c) \qquad [23]$$

where Iv is the Ivantsov function, T_∞ is the melt temperature far from the tip, and C_0 is the initial composition of alloys. Rewriting Eqs. [22] and [23], the interfacial temperature T_i and the liquid composition at the interface C^*_l can be given as

$$T_i = T_\infty + \frac{\Delta H_f}{C_p}\mathrm{Iv}(P_t) \qquad [24]$$

$$C^*_l = \frac{C_0}{1-(1-k)\mathrm{Iv}(P_c)} \qquad [25]$$

As defined explicitly in the DA model,[8] the present work also considers the four parts of bath undercooling (ΔT): the curvature undercooling ($\Delta T_r = 2\Gamma/r$), the thermal undercooling ΔT_t defined by $T_i - T_\infty$, the constitutional undercooling ΔT_c determined by $T_l(C_0) - T_l(C^*_l)$ (T_l is the liquidus temperature), and the kinetic undercooling ΔT_k.

Up to now, the entire model has been established. In the present model, the interface migration velocity V, the radius of curvature at the dendritic tip r, the interfacial temperature T_i, and the solute concentrations at the interface C^*_s and C^*_l are chosen as five independent variables. These variables can be uniquely determined by solving the set of equations including Eqs. [4], [18], [20], [24], and [25] with the iteration method, for a given alloy system at a given bath undercooling ΔT (or T_∞).

III. COMPARATIVE ANALYSIS

In order to make a comparison between the present model and Wang *et al.*'s model, the Pb-Sn alloy, a typical eutectic system, was adopted in the computations. The detailed comparative analysis of Wang *et al.*'s model and the previous models can been found in Reference 14. The free energy functions of solid and liquid phases are required as a main input, which are described by the temperature-dependent subregular solution model:[32]

$$G^i(X,T) = (1-X)G^i(0,T) + XG^i(1,T) + \mathrm{R_g}T[X\ln X + (1-X)\ln(1-X)] + X(1-X)[\Omega^i_0 + \Omega^i_1(2X-1)] \qquad [26]$$

where X is the mole fraction of Pb, T is the temperature (Kelvin), the superscript i denotes the solid phase (α, with BCT structure) or liquid phase (L), and the Ω terms are the interaction parameters. The related thermodynamic parameters are given in Table I. The thermodynamic model and the parameters are well based on Fecht *et al.*'s experimental results[32] and optimized using the CALPHAD (calculation of phase diagram) method.[33] Other parameters used in the model computations are given in Table II. In addition, the hypercooling $\Delta H_f/C_p$ is calculated with classical thermodynamic formulas based on the free energy data from Table I. As shown in Figure 1, it is variable with temperature.

Table I. Thermodynamic Parameters Used in Computations of the Interfacial Driving Force for the Pb-Sn System

Parameter	Value (J/mole)
$G^\alpha(0,T) - G^L(0,T)$	$-7103.1 + 14.0807T - 1.47031 \times 10^{-18}T^7$
$G^\alpha(1,T) - G^L(1,T)$	$-4183.13 + 11.2704T + 6.019 \times 10^{-19}T^7$
Ω^α_0	$19,692.5 - 15.8939T$
Ω^α_1	0
Ω^L_0	$5367.64 + 0.93408T$
Ω^L_1	$97.81 + 0.09353T$

Table II. Thermophysical Data Used in Model Computations[8,13]

Parameter	Value		Unit
	Pb-Sn	$Cu_{70}Ni_{30}$	
Capillarity constant Γ	1.0×10^{-7}[8]	1.3×10^{-7}[13]	Km
Thermal diffusivity α	1.7×10^{-5}[8]	4.5×10^{-6}*	m^2/s
Diffusion coefficient $D = D_0 \exp(-Q/R_g T)$	$D_0 = 2 \times 10^{-7}$[8]	$D_0 = 1.5 \times 10^{-7}$*	m^2/s
	$Q = 20,000$[8]	$Q = 40,630$*	J/mol
Interface diffusion speed V_{DI}	2.6[8]	19[13]	m/s
Diffusion speed in bulk liquid V_D	10*	20[13]	m/s
Maximum solidification rate V_0	500[8]	553[13]	m/s
Sites fraction f	1*	0.65*	—
Gas constant R_g	8.314	8.314	J/mol K

*Present work.

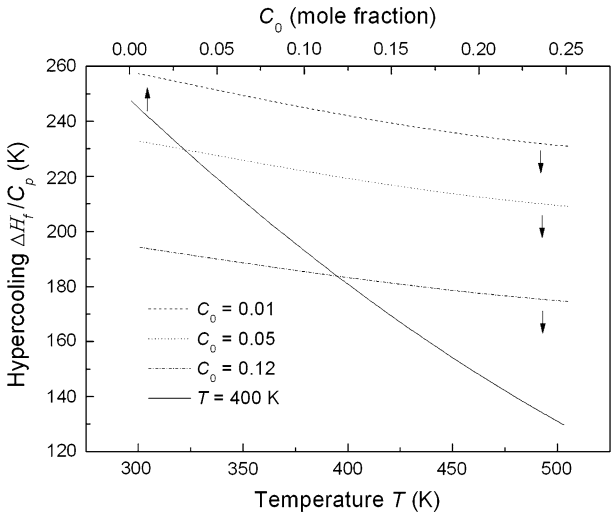

Fig. 1—Values of hypercooling $\Delta H_f/C_p$ used in model computations as a function of temperature T and alloy composition C_0.

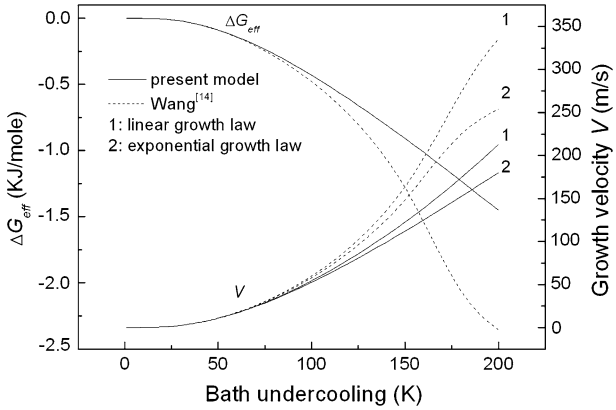

Fig. 2—Interfacial driving force ΔG_{eff} and growth velocity *vs* bath undercooling, calculated by the present model and Wang *et al.*'s model[14] for $C_0 = 0.01$.

The calculated model predictions with different nominal compositions of alloys, C_0, are shown in Figures 2 through 5. The driving force is calculated without solute drag ($\gamma = 0$). Introducing γ makes it possible to readily discuss the influence of solute drag on the solidification behavior and to search the solute drag effect. Based on the present model, these works were carried out applying to Pb-Sn and Si-As systems. The corresponding study for the diffusive interface model applicable to concentrated alloys should also be undertaken. However, these studies are out of the scope of the present article and will be published elsewhere.

Figure 2 shows the effective driving force ΔG_{eff} as a function of the bath undercooling for $C_0 = 0.01$, *i.e.*, dilute alloys. The difference increases with the undercooling, and it is significant at high undercoolings. The difference of ΔG_{eff} includes two parts. Part one comes from the approximation to the realistic thermodynamic driving force by using the Baker–Cahn equation[23] in Wang *et al.*'s model. It is well known that the Baker–Cahn equation is only suitable for an ideal solution. Part two comes from the simplification for the Baker–Cahn equation on the dilute assumption (Eqs. [3]). For a dilute solution, the ideal solution approximation is reasonable and part one of the difference is neglectable. However, part two of the difference cannot be neglected at high undercoolings. This is because Wang *et al.*'s model adopts an approximation, $\ln(1 - C_l^{eq}) \approx -C_l^{eq}$, to simplify the Baker–Cahn equation (Eq. [3]). In the equilibrium phase diagram of Pb-Sn alloy, it can be clearly explicated that below the eutectic temperature, this approximation is not suitable at all. Therefore, even for dilute alloys, Wang *et al.*'s model is not suitable to high undercoolings. As for concentrated alloys, computation indicates that part one of the difference also appears owing to the ideal solution approximation in Wang *et al.*'s model.

From Turnbull's growth law (Eq. [4]), the tip velocity is strongly dependent on the driving force. This phenomenon is also illustrated in Figure 2. For these two models, velocities are calculated by using both linear $(\Delta G_{eff}/R_g(T_i + \Delta T_r) + V/fV_0 = 0)$ and exponential growth laws to show the divergence resulting from the linear approximation in Wang *et al.*'s model. In this figure, it can be found that at high undercoolings, the values of V/fV_0 ($V_0 = 500$ m/s and $f = 1$) reach about 0.5. Thus, the linear approximation $\ln(1 - V/fV_0) \sim -V/fV_0$ is also not suitable at high undercoolings.

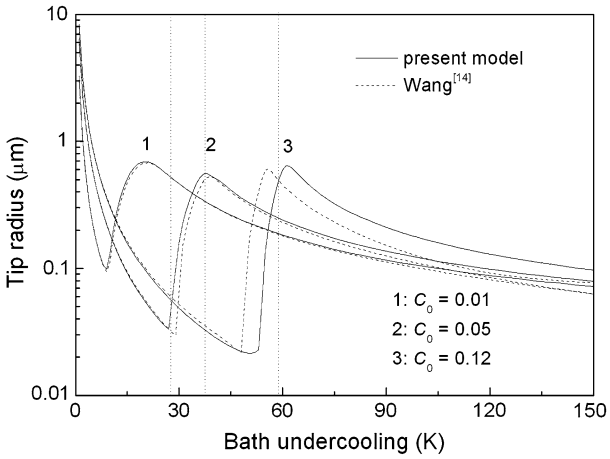

Fig. 3—Tip radius *vs* bath undercooling, calculated by the present model and Wang *et al.*'s model[14] for different C_0. The different solidification regimes are separated into four regions shown at the curves for C_0 = 0.05. These regions indicate the mainly diffusion-controlled, the transition, and the mainly and purely thermal-controlled regimes, respectively, from low to high undercoolings.

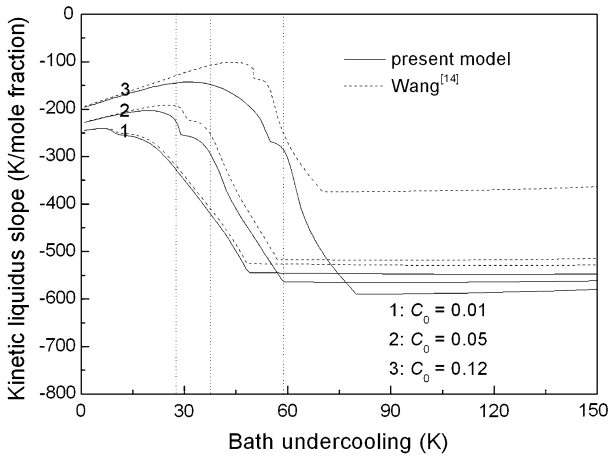

Fig. 4—Relationship between the kinetic liquidus slope M and bath undercooling, calculated by the present model and Wang *et al.*'s model[14] for different C_0. The vertical dot lines are the same as that in Fig. 2.

The tip radius as a function of the bath undercooling is shown in Figure 3. Compared with the present model, Wang *et al.*'s model has a transition region that moves rightward for $C_0 = 0.05$ and moves leftward for $C_0 = 0.12$, while for $C_0 = 0.01$, the results for both models are similar. Furthermore, computation indicates that the positions of the transition region are also similar for both models at about 0.09 for C_0. This is just a coincidence. Through numerical analysis, it was concluded that the interesting phenomenon is attributed to two main factors. The first is that Wang *et al.*'s model universally overestimates the kinetic liquidus slope M (Figure 4). From Eq. [18], the increase of M advances the diffusion-controlled regime. The second one is that Wang *et al.*'s model overestimates the tip velocity (Figure 2), particularly at high undercoolings. It is well known that the high solidification velocity suppresses the solute diffusion and accelerates the solute trapping

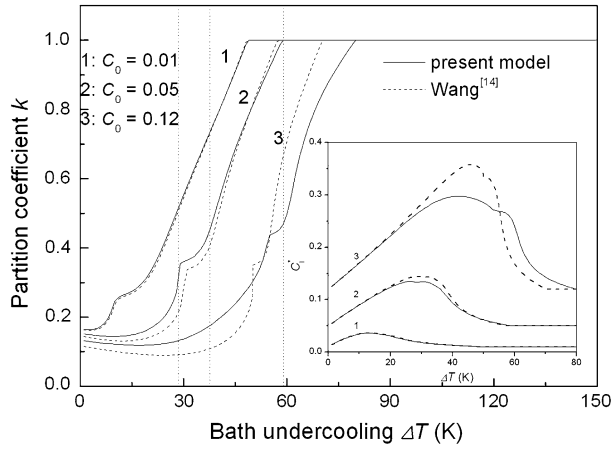

Fig. 5—Nonequilibrium partition coefficient k *vs* bath undercooling ΔT, calculated by the present model and Wang *et al.*'s model[14] for different C_0. The insert is the liquid composition C_l^* at the interface as a function of ΔT. The vertical dot lines are the same as that in Fig. 2.

to occur. Thus, the two opposite factors compete with each other and result in the interesting phenomenon.

The relationship between the nonequilibrium partition coefficient k and the bath undercooling ΔT is shown in Figure 5. The interfacial liquid solute concentration C_l^* *vs* ΔT is shown in the insert. It implies that the significant disagreement for k occurs mainly at undercoolings where C_l^* values are larger than 0.1. This can be understood through comparing the solute trapping equations used in both models. For Wang *et al.*'s model (Eqs. [19]), the simplification lies in omitting the term $(1 - \kappa_e')C_l^*$ in Eq. [20a], except replacing κ_e' by k_e'. Therefore, it is the simplification with the dilute alloy assumption that brings the significant divergence for k when C_l^* is larger than 0.1.

From the results of model computations, it should also be highlighted that the difference of the model predictions for both models increases with the nominal composition C_0, by reason of the inherent limitation of dilute alloys in Wang *et al.*'s model. So, it is necessary to examine the applicability of the present model to nondilute alloys. A comparison with the available experimental data for $Cu_{70}Ni_{30}$ alloy was made. The thermodynamic model and data are from References 34 and 35 for computation and optimization of the Cu-Ni phase diagram. The related values of the parameters used in the model computation are also given in Table II. Figure 6 shows the data points from the electromagnetic levitation experiment,[9] and the calculated dendritic growth velocity as a function of the bath undercooling for the present model, with ($\gamma = 0$) and without ($\gamma = 0$) solute drag, and Wang *et al.*'s model. As can be seen clearly, the present model with solute drag can give a satisfactory agreement with the experimental data.

IV. SUMMARY

A steady-state free dendritic growth model applicable to concentrated alloys was developed as an extension of

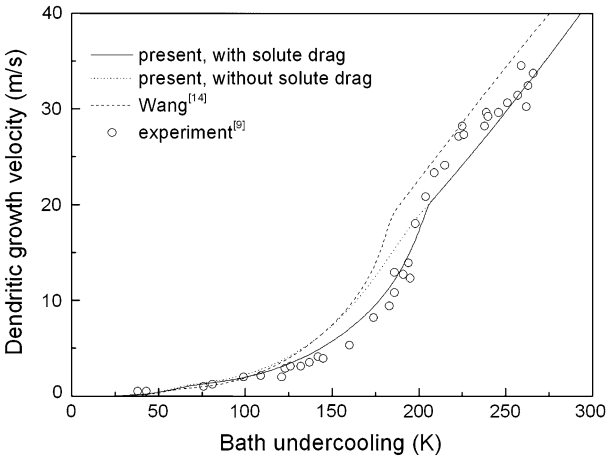

Fig. 6—Calculated (curves) and experimental[9] (open circle) dendritic growth velocities *vs* the bath undercooling for $Cu_{70}Ni_{30}$ alloy. The parameter f is assumed to be 0.65 to obtain the best description of the experimental results.

Wang *et al.*'s model.[14] The present model adopted a reasonable thermodynamic model to replace the Baker–Cahn equation and included a generalized marginal stability criterion and a nondilute solute trapping model to completely eliminate the dilute alloy limitation. It was concluded by a comparative analysis that the difference between the present model and Wang *et al.*'s model increases with the nominal composition of alloys due to the inherent dilute limitation in Wang *et al.*'s model. Furthermore, Wang *et al.*'s model has a reasonable approximation to the present model at low undercoolings for a dilute alloy. However, the discrepancy appears at high undercoolings even for dilute alloys. A comparison with the available experimental data demonstrates the applicability of the present model to nondilute alloys.

ACKNOWLEDGMENTS

The authors are grateful to Professor Teiichi Ando for the valuable discussion of this work. The constructive suggestions of Peter Galenko as well as the helpful comments of Haifeng Wang and Feng Liu on the manuscript are kindly acknowledged. The work was supported by the National Natural Science Foundation of China (Grant Nos. 51074112 and 51101046), the Key Program of the Tianjin Natural Science Foundation (Grant No. 11JCZDJC22100), and the Scientific Research Fund of the Heilongjiang Provincial Education Department (Grant No. 12511073).

REFERENCES

1. D.M. Herlach: *Mater. Sci. Eng. R*, 1994, vol. 12, pp. 177–272.
2. W.J. Boettinger, S.R. Coriell, A.L. Gereer, A. Karma, W. Kurz, M. Rappaz, and R. Trivedi: *Acta Metall.*, 2000, vol. 48, pp. 43–70.
3. F. Liu and G.C. Yang: *Int. Mater. Rev.*, 2006, vol. 51, pp. 145–70.
4. J. Lipton, M.E. Glicksman, and W. Kurz: *Mater. Sci. Eng.*, 1984, vol. 65, pp. 57–63.
5. J. Lipton, W. Kurz, and R. Trivedi: *Acta Metall.*, 1987, vol. 35, pp. 957–64.
6. R. Trivedi, J. Lipton, and W. Kurz: *Acta Metall.*, 1987, vol. 35, pp. 965–70.
7. W.J. Boettinger, S.R. Coriell, and R. Trivedi: in *Rapid Solidification Processing: Principles and Technologies IV*, R. Mehrabian, and P.A. Parrish, eds., Claitor's Publishing Division, Baton Rouge, LA, 1988, pp. 13–25.
8. A.G. Divenuti and T. Ando: *Metall. Mater. Trans. A*, 1998, vol. 29A, pp. 3047–56.
9. R. Willnecker, D.M. Herlach, and B. Feuerbacher: *Appl. Phys. Lett.*, 1990, vol. 56, pp. 324–26.
10. K. Eckler, R.F. Cochrane, D.M. Herlach, B. Feuerbacher, and M. Jurisch: *Phys. Rev. B*, 1992, vol. 45, pp. 5019–22.
11. C.B. Arnold, M.J. Aziz, M. Schwarz, and D.M. Herlach: *Phys. Rev. B*, 1999, vol. 59, pp. 334–43.
12. D. Jou, J. Casas-Vazquez, and G. Lebon: *Rep. Prog. Phys.*, 1999, vol. 62, pp. 1035–1142.
13. P.K. Galenko and D.A. Danilov: *J. Cryst. Growth*, 1999, vol. 197, pp. 992–1002.
14. H.F. Wang, F. Liu, Z. Chen, G.C. Yang, and Y.H. Zhou: *Acta Mater.*, 2007, vol. 55, pp. 497–506.
15. S. Li, J. Zhang, and P. Wu: *J. Cryst. Growth*, 2010, vol. 312, pp. 982–88.
16. S. Li, J. Zhang, and P. Wu: *Scripta Mater.*, 2009, vol. 61, pp. 485–88.
17. S. Önel and T. Ando: *Metall. Mater. Trans. A*, 2008, vol. 39A, pp. 2449–58.
18. H. Hartmann, P.K. Galenko, D. Holland-Moritz, M. Kolbe, D.M. Herlach, and O. Shuleshova: *J. Appl. Phys.*, 2008, vol. 103, p. 073509.
19. P.K. Galenko: *Phys. Rev. B*, 2002, vol. 65, p. 144103.
20. M.J. Aziz and T. Kaplan: *Acta Metall.*, 1988, vol. 36, pp. 2335–47.
21. M. Hillert: *Acta Mater.*, 1999, vol. 47, pp. 4481–4505.
22. S. Li, J. Zhang, and P. Wu: *Scripta Mater.*, 2010, vol. 62, pp. 716–19.
23. J.C. Baker and J.W. Cahn: *Solidification*, ASM, Metals Park, OH, 1971, pp. 23–58.
24. D. Turnbull: *J. Phys. Chem.*, 1962, vol. 66, pp. 609–13.
25. J.S. Langer and H. Muller-Krümbhaar: *Acta Metall.*, 1978, vol. 26, pp. 1681–87.
26. R. Trivedi and W. Kurz: *Acta Metall.*, 1986, vol. 34, pp. 1663–70.
27. P.K. Galenko and D.V. Danilov: *Phys. Rev. E*, 2004, vol. 69, p. 051608.
28. S.L. Sobolev: *Phys. Rev. E*, 1997, vol. 55, pp. 6845–54.
29. P.K. Galenko: *Phys. Rev. E*, 2007, vol. 76, p. 031606.
30. G.P. Ivantsov: *Dokl Akad Nauk SSSR*, 1947, vol. 58, pp. 567–69.
31. G.P. Ivantsov: *Dokl Akad Nauk SSSR*, 1952, vol. 83, pp. 573–76.
32. H.J. Fecht, M.X. Zhang, Y.A. Chang, and J.H. Perepezko: *Metall. Trans. A*, 1989, vol. 20A, pp. 795–803.
33. U.R. Kattner: *JOM*, 1997, vol. 49 (12), pp. 14–19.
34. S. An Mey and R.W.T.H. Aachen: *CALPHAD*, 1992, vol. 16, pp. 255–60.
35. X.Y. Yan, Y.A. Chang, Y. Yang, F.Y. Xie, S.L. Chen, F. Zhang, S. Daniel, and M.H. He: *Intermetallics*, 2001, vol. 9, pp. 535–38.